Chapter 2
Spectral Image Acquisition

Throughout the book, we make very little, if any, differentiation between the use of spectra in the visible, ultraviolet and near-infrared ranges. This is because applications of imaging spectroscopy for scene understanding using benchtop hyperspectral and multispectral cameras are not necessarily constrained to the range visible to the human eye.

Moreover, we will often refer to the electromagnetic radiation in terms of its wavelength. In particular we will focus on wavelengths spanning from the ultraviolet (UV) to the infrared in its A and B bands (IR-A and IR-B). Here, we use the naming convention of the International Commission on Illumination (CIE) in preference over that proposed by the International Organization for Standardization (ISO). In Table 2.1, we summarise the two main subdivisions of the spectrum, i.e. those corresponding to the CIE and the ISO.

As mentioned earlier, a hyperspectral or multispectral image comprises a set of wavelength indexed bands sampled over a spectral range. In Fig. 2.1, we show the electromagnetic spectrum, divided following the CIE standards, and illustrate how a landscape appears at different bands. As illustrated in Fig. 1.2, the appearance of the scene shows noticeable changes with respect to wavelength.

Since every pixel in the image accounts for a set of wavelength resolved measurements, the acquisition process across the spectral range greatly depends on the camera used to capture the image. Furthermore, the sensor itself may require calibration to account for noise and bias. In this section, we provide an overview of the existing spectral imaging technologies, reduction of the camera sensor noise and rectification of the image spectra with respect to the illumination.

2.1 Spectral Cameras and Sensors

Although imaging spectroscopy has been available as a remote sensing technology since the 1960s, until recently, commercial spectral imaging systems were mainly airborne ones which could not be used for ground-based image acquisition. Furthermore, spectral imaging has often only been available to a limited number of

A. Robles-Kelly, C.P. Huynh, *Imaging Spectroscopy for Scene Analysis*,
Advances in Computer Vision and Pattern Recognition, DOI 10.1007/978-1-4471-4652-0_2,

Table 2.1 Spectral subdivisions according to the CIE and the ISO

Ultraviolet				
ISO[a]	UV-C (100–280 nm)	UV-B (280–315 nm)	UV-A (315–400 nm)	
CIE[b]	UV-C (100–280 nm)	UV-B (280–315 nm)	UV-A1 (315–340 nm)	UV-A2 (340–400 nm)
Visible				
ISO				VIS (400–780 nm)
CIE				VIS (400–700 nm)
Infrared				
ISO[c]	Near-Infrared (780 nm–3 µm)		Mid-Infrared (3–50 µm)	Far-Infrared (50 µm–1 mm)
CIE	IR-A (700 nm–1.400 µm)	IR-B (1.4–3 µm)	IR-C (3 µm–1 mm)	

[a]See ISO-DIS-21348 and, for the infrared range, see ISO 20473:2007

[b]See 134/1 TC 6-26 report: Standardization of the Terms UV-A1, UV-A2 and UV-B

[c]See ISO 20473:2007

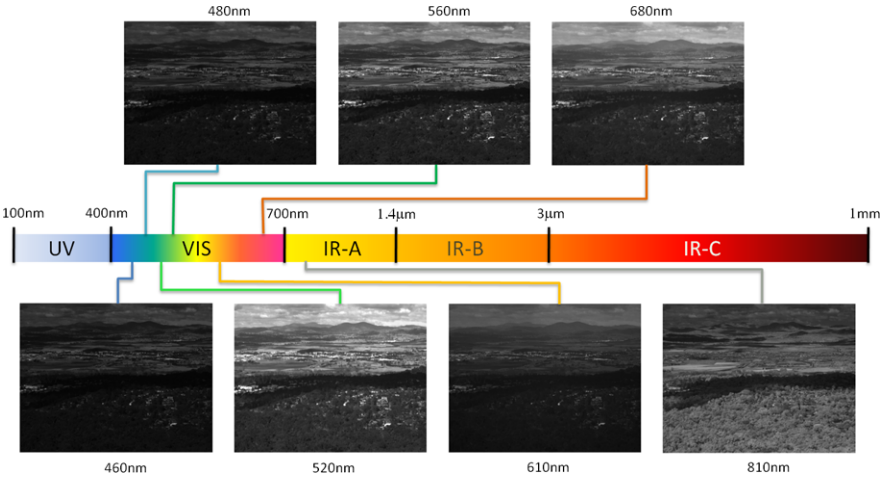

Fig. 2.1 The ultraviolet, visible and infrared spectrum as related to the wavelength resolved bands corresponding to a spectral image of a landscape

researchers and professionals due to the high cost of spectral cameras and the complexity of processing spectral data corresponding to large numbers of bands.

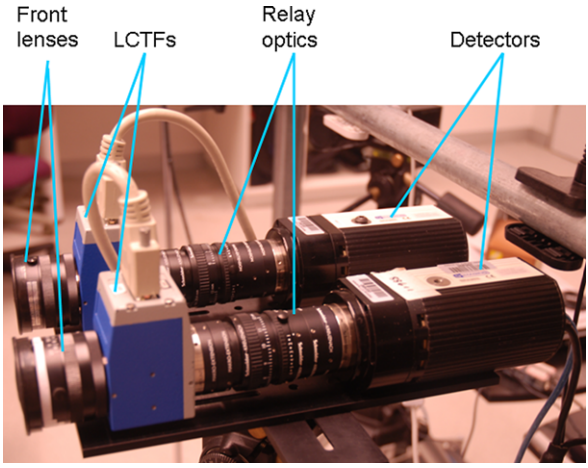

Fig. 2.2 An example benchtop camera system with two sets of filters, optics and detectors (one for the near-infrared and the other one for the visible range). The cameras are connected in daisy chain

At present, remote sensing imaging technologies coexist with ground-based commercial systems based on liquid crystal tunable filters (LCTFs), acousto-optic tunable filters (AOTFs), Fabry–Perot imagers and multiple-CCD cameras. These technologies comprise the staring arrays, pushbrooms and multiple-CCD spectral cameras used today.

Pushbroom imagers are so named since they gather all of the spectrum at a time for a line on the image. This sequential line acquisition has been used in both remote sensing and benchtop cameras. In a pushbroom imager, the incoming light is gathered by a collimating slit and projected onto a diffraction grating. The diffraction grating disperses the spectrum across the detectors. The main advantage of pushbroom imagers is the fact that all of the spectrum is acquired at the same time. The drawback is that, since one line of the image is acquired at every scan, either the camera or the object should move accordingly. This is, in itself, not a major issue for applications such as remote sensing or industrial machine vision, where the camera is mounted on a moving satellite, a processing line or conveyor belt.

In contrast, staring arrays are band-sequential imagers. That is, the scene is acquired at full spatial resolution at one wavelength indexed band at a time. In a staring array device, the light passes through the focusing optics and then it is filtered, so only a narrowband segment of the spectrum impinges on the focal plane of the sensor, which is typically a CCD. In some cases, a set of relay optics is included to avoid undesired distortions induced by the filters. These filters can be fixed ones mounted on a revolving disk or tunable filters. An example of a staring array camera system is shown in Fig. 2.2. Note that the system comprises the focusing optics, the tunable filters, which in this case are LCTFs, relay optics and a detector built upon a CCD. The figure shows two cameras in daisy chain, one of which operates in the near-infrared range, whereas the other is devoted to the visible range.

It is worth noting that tunable filters in staring array devices are predominantly based on acousto-optic or liquid crystal technologies. AOTFs are solid state optical devices consisting of a tellurium dioxide (TeO_2) or quartz crystal attached to a

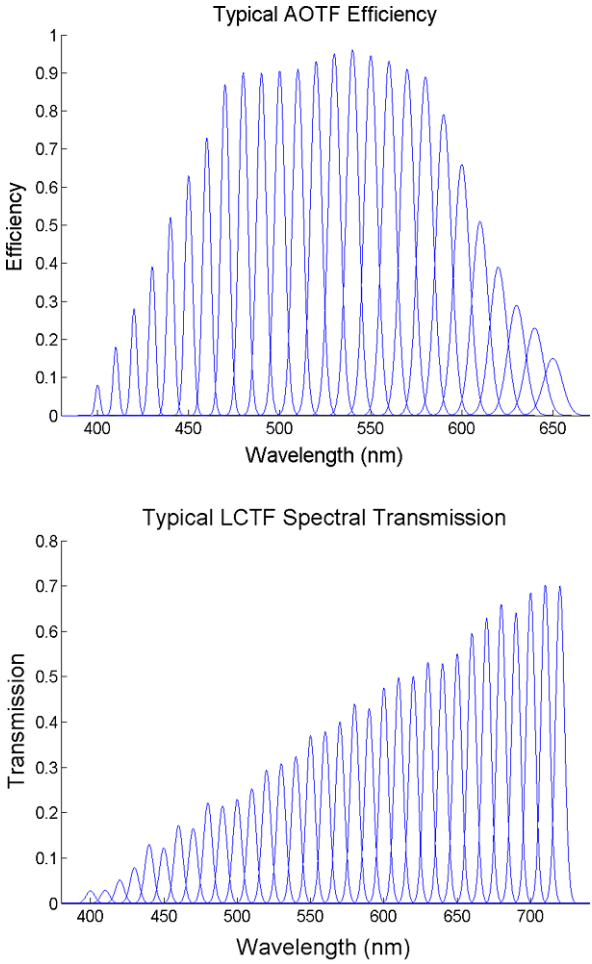

Fig. 2.3 *Top*: typical transmission as a function of wavelength for an acousto-optic tunable filter; *Bottom*: typical transmission for a liquid crystal tunable filter

transducer. When a radio frequency signal is applied to the transducer, a high frequency acoustic wave ensues and propagates through the crystal. This ultrasonic acoustic wave induces a change in the refractive index that acts as a transmission diffraction grating. As a result, in practise, the selectivity of the filter is often not fixed across the spectral range. In Fig. 2.3, we show the typical transmission for an AOTF. In the figure, we have tuned the filter to 10 nm intervals. In particular, note that the selectivity of the filter widens as it progresses towards the upper end of the spectrum.

In contrast, LCTFs are based on a set of liquid crystal wave plates (liquid crystal-linear polariser interwoven combinations). In contrast with AOTFs, because they use wave plates rather than being based on changes in the index of refraction, LCTFs provide a linear optical path, which delivers a very low distortion and, hence, high image quality. Thus, intuitively, LCTFs can be viewed as a stack of non-tunable

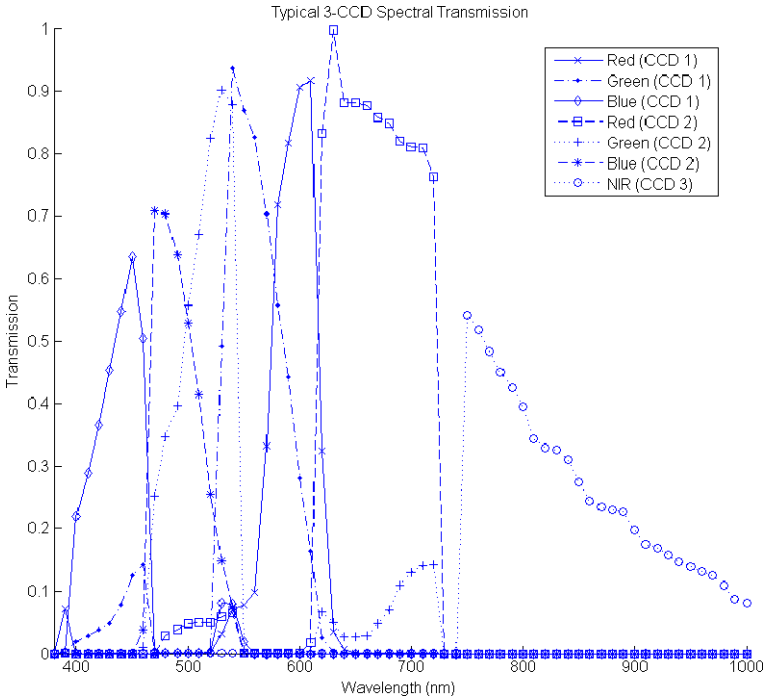

Fig. 2.4 Typical spectral transmission for a seven-band multiple-CCD camera

filters which can be set to on/off states. As a result, they can only be tuned to set intervals. In contrast, AOTFs, in theory, may be tuned to any wavelength across their operating range due to the fact that they effectively operate on an acoustic wave generated by the transducer attached to the quartz or TeO_2 crystal. On the other hand, the use of wave plates with linear polarisers often implies low filter transmissions compared to those of AOTFs. In Fig. 2.4, we show the filter transmission as a function of wavelength. Again, we have tuned the filter at 10 nm intervals. Note that the selectivity of the filter is unchanged with respect to wavelength.

Whereas AOTFs and LCTFs are often employed in hyperspectral cameras, for multispectral imaging, multiple-CCD cameras provide the ability to capture the full set of spectral bands at all pixels in the image at the same time. Multiple-CCD cameras employ a set of beam splitting prisms to separate the light incoming through the lens. The use of multiple CCDs and prisms implies that the complexity of the camera becomes impractical for a large number of bands. Nonetheless, for a few wavelength-resolved bands, multiple-CCD imaging systems provide the capability for "single shot" multispectral acquisition. In Fig. 2.4 we show the typical spectral transmission for a seven-band three-CCD camera. Note that the transmission is not reminiscent of a Gaussian band-pass filter anymore, but rather is a non-linear combination of the beam splitting prism selectivity and the Bayer array on the CCD.

2.2 Dark Current Calibration

Regardless of the method used to separate the incoming light into a set of wavelength indexed bands, hyperspectral and multispectral imaging technologies make use of detectors based on CCDs. The main reason for this is their high quantum efficiency, i.e. the charge per photon impinging on the detector. Nonetheless, CCDs suffer from photon, thermal and read noise. This is particularly important in hyperspectral and multispectral image acquisition since the spectral power per band can be, potentially, quite low due to the narrow nature of the transmission function for the spectral filters.

Recall that, for a CCD, the detector output signal can be expressed as

$$\mathcal{O} = (\mathcal{P}Q_e + \mathcal{D})t + \mathcal{R}, \tag{2.1}$$

where $\mathcal{P}$ is the incident photon flux (photons per detector over second), Q_e is the quantum efficiency, $\mathcal{D}$ is the thermal noise, $\mathcal{R}$ is the read noise, i.e. bias, and t is the exposure time.

Since thermal noise accounts for electrons thermally generated within the CCD, it is present even when the shutter is closed and no light is impinging on the detector. As a result, it is also often called the dark current of the sensor. In practise, at acquisition time, this can be removed by taking an image with the shutter closed, i.e. $\mathcal{P} = 0$ over a set integration time t_0. This yields the dark image output given by

$$\mathcal{O}_D = \mathcal{D}t_0 + \mathcal{R}. \tag{2.2}$$

Since spectral imaging technologies often employ high-performance CCDs which exhibit a negligible read noise, we can remove $\mathcal{R}$ from further consideration and use the shorthand $\mathcal{D} \approx \frac{\mathcal{O}_D}{t_0}$. This permits the subtraction of the dark image output from the detector output signal, which yields

$$\mathcal{P}Q_e t \approx \mathcal{O} - \frac{t}{t_0}\mathcal{O}_D, \tag{2.3}$$

which implies that, if the quantum efficiency of the sensor is known, the incident photon flux can be approximated using the expression

$$\mathcal{P} \approx \frac{1}{Q_e t}\left(\mathcal{O} - \frac{t}{t_0}\mathcal{O}_D\right). \tag{2.4}$$

Thus, by effecting the dark image output subtraction we are effectively performing a calibration against noise. Throughout the remainder of this book, we will assume that this dark image calibration has been effected at acquisition time. Further, after calibration, for narrowband filters, we can view the image intensity value $I(u, \lambda)$ at pixel u and wavelength λ as the quantity in Eq. (2.3) weighted by the filter transmission. Thus, we can write

$$I(u, \lambda) = \beta_\lambda\left(\mathcal{O} - \mathcal{O}_D\frac{t}{t_0}\right) \approx \beta_\lambda Q_e \mathcal{P}t, \tag{2.5}$$

where β_λ is a wavelength-dependent quantity that depends on the geometry of the sensor and the spectral transmission of the optical filter or grating used in the imager.

2.3 Notes

In this chapter, we have focused on the image acquisition process. This is relevant to the exposure time and shutter speed, which are of major importance to capture spectral and trichromatic imagery. Exposure settings usually determine how much, and for how long, light should be allowed to reach the imaging sensors. This is intrinsically linked to the sensitivity of the sensors.

It is also important to understand that natural scenes can vary from very low to very high luminous intensities. The developments presented here have been, so far, devoid of considerations regarding the dynamic range of the sensor, i.e. the ratio between the maximum and minimum intensity value delivered by the imager. In practise, the dynamic range should be taken into consideration and the exposure time should be set carefully, since high contrast may potentially deliver images with reduced dynamic range. Thus, there is a trade-off to be made with respect to the contrast in the image.

http://www.springer.com/978-1-4471-4651-3

Imaging Spectroscopy for Scene Analysis

Robles-Kelly, A.; Huynh, C.P.
2013, XVIII, 270 p., Hardcover
ISBN: 978-1-4471-4651-3